Draft version January 4, 2023
Typeset using LaTeX **twocolumn** style in AASTeX631

Towards ultra metal-poor DLAs: linking the chemistry of the most metal-poor DLA to the first stars

Louise Welsh [1,2] Ryan Cooke [3] Michele Fumagalli [1,4] and Max Pettini [5]

[1] *Dipartimento di Fisica G. Occhialini, Università degli Studi di Milano Bicocca, Piazza della Scienza 3, I-20126 Milano, Italy*
[2] *INAF – Osservatorio Astronomico di Brera, via Bianchi 46, I-23087 Merate (LC), Italy*
[3] *Centre for Extragalactic Astronomy, Durham University, South Road, Durham DH1 3LE, UK*
[4] *INAF - Osservatorio Astronomico di Trieste, via G. B. Tiepolo 11, I-34143 Trieste, Italy*
[5] *Institute of Astronomy, University of Cambridge, Madingley Road, Cambridge CB3 0HA, UK*

ABSTRACT

We present new Keck/HIRES data of the most metal-poor damped Lyα (DLA) system currently known. By targeting the strongest accessible Fe II features, we have improved the upper limit of the [Fe/H] abundance determination by $\sim$ 1 dex, finding [Fe/H] < -3.66 (2σ). We also provide the first upper limit on the relative abundance of an odd-atomic number element for this system [Al/H] < -3.76 (2σ). Our analysis thus confirms that this $z_{\rm abs} \simeq 3.07$ DLA is not only the most metal-poor DLA but also the most iron-poor DLA currently known. We use our stochastic chemical enrichment model, alongside the chemistry of this DLA and the yields from nucleosynthetic models, to probe its enrichment history. We find that this DLA is best modelled by the yields of an individual Population III progenitor rather than multiple Population III stars. We then draw comparisons with other relic environments and, particularly, the stars within nearby ultra-faint dwarf galaxies. We find that a star within Böotes II, that showcases a similar chemistry to that of the DLA presented here, may have been enriched by a progenitor with similar properties. This metal-poor DLA, observed ~ 2 Gyrs after the Big Bang, thus acts as a beacon to some of the least polluted gas in the early Universe.

Keywords: Damped Lyman-alpha systems (349); Intergalactic medium (813); Population III stars (1285); Population II stars (1284); Chemical abundances (224)

1. INTRODUCTION

Tracing chemical evolution from the Cosmic Dawn at $z \sim 15 - 30$ to the present epoch will reveal how the Universe transformed from primordial gas (i.e. primarily hydrogen and helium) to the complex composition of chemical elements we observe locally. Our current understanding suggests that the first generation of stars (known as Population III, or Pop III stars) were the catalysts of this process in the early Universe (see e.g. Bromm & Yoshida 2011). Since the properties of these stars remain elusive to observations, the relative quantities of metals that they produced is also an open question. To understand the earliest epochs of chemical enrichment, we must uncover the properties of the first stars.

Corresponding author: Louise Welsh
louise.welsh@unimib.it

Observationally, we have searched for these stars in the local Universe for over four decades (e.g. Bond 1980; Beers et al. 1985; Ryan et al. 1991; Beers et al. 1992; McWilliam et al. 1995; Ryan et al. 1996; Cayrel et al. 2004; Beers & Carollo 2008; Christlieb et al. 2008; Roederer et al. 2014; Howes et al. 2016; Starkenburg et al. 2017). None have been found. In the future, if the lack of detections persist, it may be possible to empirically rule out Population III properties (e.g. the slope or shape of the initial mass function; IMF) through these non-detections (Hartwig et al. 2015).

Cosmological hydrodynamic simulations that follow the formation of Pop III stars from cosmological initial conditions suggest that the first stars were more massive than the Sun, with typically masses between $10 < M/{\rm M}_{\odot} < 100$ (Tegmark et al. 1997; Barkana & Loeb 2001; Abel et al. 2002; Bromm et al. 2002; Turk et al. 2009; Greif et al. 2010; Clark et al. 2011; Hirano et al. 2014; Stacy et al. 2016). If Pop III stars really were limited to these mass scales, their short lifetimes

mean they may only be visible at very high redshift; directly observing the supernovae of these stars is one of the flagship goals of the recently launched James Webb Space Telescope (JWST). This facility provides a new avenue to observationally investigate the first stars and galaxies which may revolutionise this field in the coming years (Gardner et al. 2009). A complementary approach to searching for these stars directly is to search for the elements that they produced.

Reservoirs of gas, detected as absorption along the line-of-sight towards unrelated background quasars, are reliable probes of cosmic chemical evolution. These low density structures allow us to trace the evolution of metals from $0 < z < 5$ with a consistent degree of sensitivity (Péroux & Howk 2020). The absorption line systems whose column density of neutral hydrogen exceeds $\log_{10} N(\mathrm{H\,I})/\mathrm{cm}^{-2} \geq 20.3$ are known as Damped Lyα systems (DLAs; see Wolfe et al. 2005 for a review). DLAs are uniquely suited to high-precision chemical abundance studies; the large column density of neutral hydrogen means that the gas is optically thick to ionizing radiation and the constituent metals reside primarily in a single, dominant ionization state. This negates the need for ionization corrections and, thus, the column density of the observed ionic species can be used to accurately determine the relative metal abundances of the gas reservoir. These objects are most easily studied in the redshift interval $2 < z < 3$, when the rest-frame UV lines are shifted into the optical wavelength range. However, these systems can be studied at any redshift once an appropriate sightline (e.g., a quasar) has been identified. Studies which probe $z > 6$ sightlines trace the composition of gas closer to the epoch of the Cosmic Dawn (Becker et al. 2011, 2019; Bosman et al. 2022; D'Odorico et al. 2022). However, at these redshifts it can be challenging to observe the characteristic Lyα absorption, which is required to determine the metallicity. At these redshifts, the Lyα can only be determined for proximate systems which are less frequent and suffer additional challenges due to the proximity to the background quasar (Simcoe et al. 2012; Bañados et al. 2019).

Indeed, there may be some near-pristine gaseous reservoirs in the early Universe that have been solely enriched by the supernovae (SNe) of the first stars (Erni et al. 2006; Pettini et al. 2008; Cooke et al. 2017; Welsh et al. 2019). The metallicity of these reservoirs provides an indication of the level of enrichment the gas has experienced from stellar populations. In principle, this property is easily defined as the the amount of metals in the system relative to the hydrogen content. This is often expressed as [X/H][1]. However, the metal (or combination of metals) used in this expression is dependent on the system being analysed and, ultimately, on the accessible features.

A typical metallicity tracer is often [Fe/H]; anything that is 1000 times more Fe-poor than the Sun (i.e. [Fe/H] < -3) is considered extremely metal-poor (EMP). While an environment that is 10 000 times more Fe-poor than the Sun (i.e. [Fe/H] < -4) is considered ultra metal-poor (UMP). As we continue to discover increasingly metal-poor objects in the low Fe-metallicity tail of the metallicity distribution, peculiar chemical abundance patterns become more apparent. The lowest Fe-metallicity environments are often associated with enhanced abundances of α-elements. This is well-documented through the analysis of metal-poor Milky Way halo stars (i.e., the stellar relics) where a deficit of Fe is frequently identified alongside an overabundance of C. These stars are known as carbon-enhanced metal-poor stars (i.e. CEMP stars; see Beers & Christlieb 2005). There have been reports of a similar carbon-enhancement in both metal-poor DLAs (Cooke et al. 2011a) and lower column density gas reservoirs (Zou et al. 2020, i.e. Lyman limit systems; LLSs — see). Though, an updated analysis of the C-enhanced DLA revealed a [C/Fe] abundance ratio more typical given the abundances observed across the metal-poor DLA population (Welsh et al. 2020). Generally, we note that when α-elements are detected in excess alongside a minimal contribution from Fe, metallicity estimates based on Fe fail to describe the overall metal-paucity of the system in question. This is worth considering when we are searching for chemically near-pristine gas.

We are yet to detect a chemically pristine DLA, although there are multiple LLSs that appear to be entirely untouched by the process of star formation (e.g. Fumagalli et al. 2011; Robert et al. 2019). There is the potential detection of an UMP DLA at $z \sim 7$ (Simcoe et al. 2012) which however hinges on the modelling of the quasar emission (see Bosman & Becker 2015) for an alternative interpretation of these data. Hence, we are also yet to firmly detect an UMP DLA. Prior to the collection of the data presented here, there have been three high-precision detections of EMP DLAs with associated errors < 0.20 (Ellison et al. 2010; Cooke et al. 2011b, 2016; Welsh et al. 2022). Rafelski et al. (2012) report a metallicity floor across DLAs of [M/H] $\simeq -3$. Thus, the detection of an UMP DLA would mark an

[1] This denotes the logarithmic number abundance ratio of elements X and H relative to their solar values $\mathrm{X}_\odot$ and $\mathrm{H}_\odot$, i.e. $[\mathrm{X/H}] = \log_{10}(N_\mathrm{X}/N_\mathrm{H}) - \log_{10}(N_\mathrm{X}/N_\mathrm{H})_\odot$.

exceptional environment. Future surveys like WEAVE, DESI, and 4MOST will provide much improved statistics, necessary to reveal where UMP DLAs lie within the population of known absorbers (Dalton et al. 2012; de Jong et al. 2012; DESI Collaboration et al. 2016; Pieri et al. 2016).

The DLA found towards the quasar SDSS J090333.55+262836.3 (hereafter J0903+2628) is the *most* metal-poor DLA currently known (Cooke et al. 2017). This was determined through the analysis of absorption from low ionic species such as C II, O I, Si II, and Fe II. The previously accessible Fe II features were restricted to the weak Fe II λ1260 transition; this was necessary to observe the absorption due to the lighter atomic number elements alongside the associated H I. Thus, these initial observations required a setup that covered blue regions of the spectrum while the strongest accessible Fe II features fall at redder wavelengths. The previous data indicate [Fe/H] < -2.81 (2σ). Given the extreme paucity of both α-elements and Fe observed for this system, we have sought additional high resolution observations that target the stronger Fe II λ1608 and Fe II λ2382 features. These observations also target the Al II λ1670 feature — providing the first insight into the abundance of odd-atomic number elements for this DLA. The results of these observations and the subsequent data analysis are the subject of this paper.

This paper is organised as follows. Section 2 describes our observations and data reduction. In Section 3, we present our data and investigate the chemical enrichment history of this system. In Section 4, we present our discussion and draw comparisons with other relic environments, before drawing overall conclusions and suggesting future work in Section 5.

2. OBSERVATIONS AND DATA REDUCTION

The DLA towards the $m_{\rm r} = 19.0$ quasar J0903+2628 at $z_{\rm em} = 3.22$ has previously been identified as the most metal-poor DLA currently known. We have acquired an additional 9 hours of echelle spectroscopic data on the associated quasar using the High Resolution Echelle Spectrometer (HIRES; Vogt et al. 1994) mounted on the 10 m Keck I telescope. These data were collected through 9×3600 s exposures across December 18$^{\rm th}$ and December 27$^{\rm th}$ 2021. We utilise the red cross-disperser to target the strongest available Fe II features that fall at red wavelengths. The data cover 5447 − 9999 Å with small wavelength gaps due to both the detector mosaic and the configuration of the instrument (that results in incomplete coverage across a small number of the reddest orders). We use the C1 decker resulting in a slitwidth = 0.861″ and a nominal resolution of $R = 49,000$ corresponding to a velocity full width at half maximum $v_{\rm FWHM} = 6.28$ km s^{-1}.

The collected data were binned 2×2 during readout. These HIRES data were reduced with the Hires REDUX[2] reduction pipeline. This pipeline includes the standard reduction steps of subtracting the detector bias, locating and tracing the echelle orders, flat-fielding, sky subtraction, optimally extracting the 1D spectrum, and performing a wavelength calibration. The data were converted to a vacuum and heliocentric reference frame.

Finally, we combined the individual exposures of this DLA using UVES_POPLER[3]. This corrects for the blaze profile, and allowed us to manually mask cosmic rays and minor defects from the combined spectrum. When combining these data we adopt a pixel sampling of 2.5 km s^{-1}.

3. ANALYSIS

Using the Absorption LIne Software (ALIS) package[4]— which uses a χ-squared minimisation procedure to find the model parameters that best describe the input data — we simultaneously analyse the full complement of high S/N and high spectral resolution data currently available for the DLA towards J0903+2628. We model the absorption lines with a Voigt profile, which consists of three free parameters: a column density, a redshift, and a line broadening. We assume that all lines of comparable ionization level have the same redshift, and any absorption lines that are produced by the same ion all have the same column density and total broadening. The total broadening of the lines includes a contribution from both turbulent and thermal broadening. The turbulent broadening is assumed to be the same for all absorption features, while the thermal broadening depends inversely on the square root of the ion mass; thus, heavy elements (e.g. Fe) will exhibit absorption profiles that are intrinsically narrower than the profiles of lighter elements, (e.g. C). The intrinsic model is then compared to the data after convolving by the line spread function of the instrument which results in an additional apparent broadening of the lines. Finally, we note that we simultaneously fit the absorption and quasar continuum. We model the continuum around every absorption line as a low-order Legendre polynomial (typically of order

[2] Hires REDUX is available from: https://www.ucolick.org/~xavier/HIRedux/.

[3] UVES_POPLER is available from: https://github.com/MTMurphy77/UVES_popler

[4] ALIS is available from: https://github.com/rcooke-ast/ALIS.

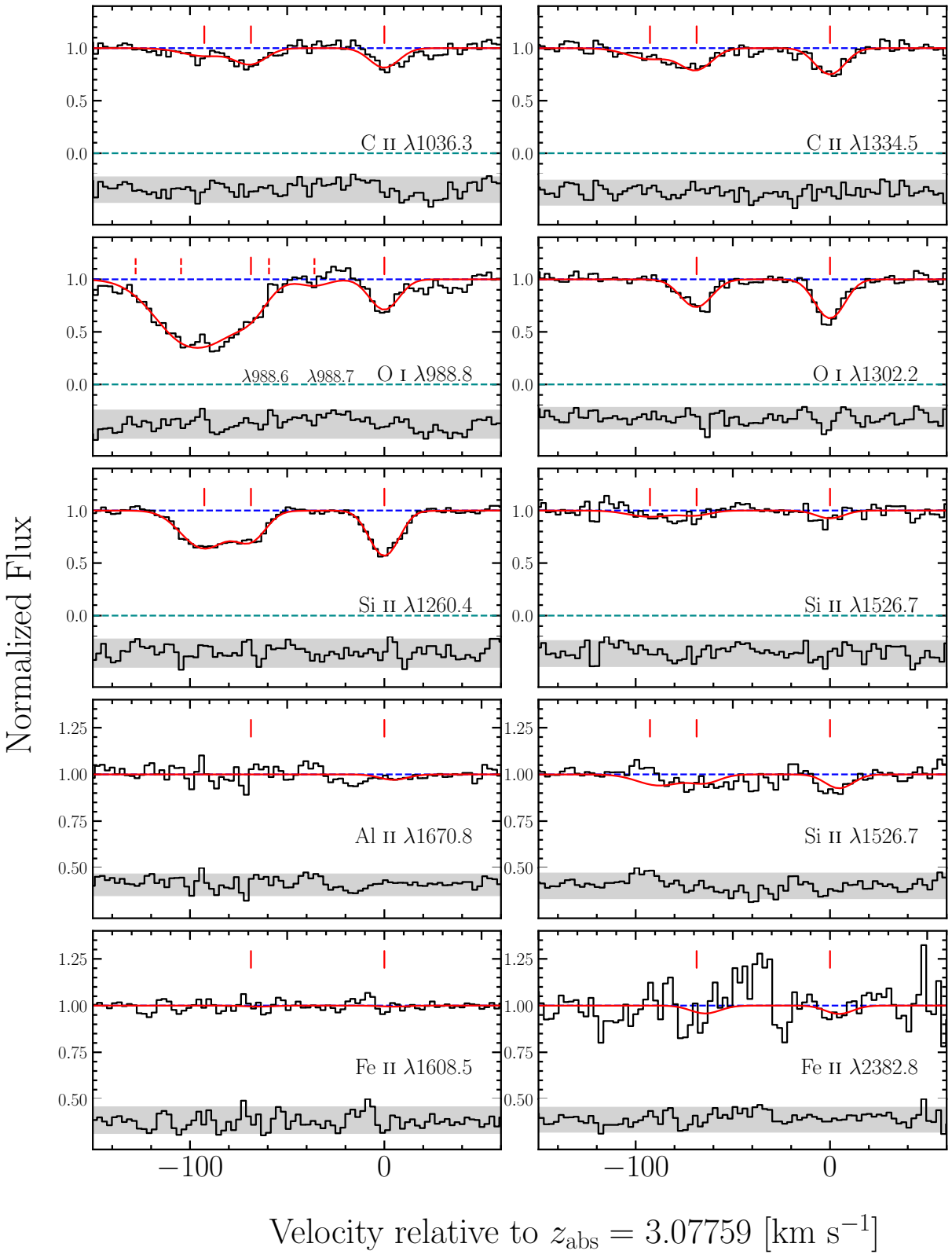

Figure 1. Continuum normalised HIRES data (black histograms) of the absorption features produced by metal ions associated with the DLA at $z_{\rm abs} = 3.077590$ towards the quasar J0903+2628. The best-fitting model is shown with the red curves. The blue dashed line indicates the position of the continuum while the green dashed line indicates the zero-level. Note the different scale of the y-axes of the bottom two rows. These bottom two rows correspond to the data collected in 2021 while the upper three rows correspond to the original Keck/HIRES data. The red ticks above the absorption features indicate the centre of the Voigt line profiles for each identified component. The dashed-red lines in the third panel highlight the additional features of the O I λ988 triplet. Below the zero-level, we show the residuals of this fit (black histogram) where the grey shaded band encompasses the 2σ deviates between the model and the data.

3). We assume that the zero-levels of the sky-subtracted HIRES data do not depart from zero[5].

The DLA towards J0903+2628 is best modelled by three absorption components for C II and Si II at redshifts $z_{\rm abs} = 3.077589 \pm 0.000002$, $z_{\rm abs} = 3.076653 \pm 0.000005$, and $z_{\rm abs} = 3.076331 \pm 0.000006$. The O I, Al II, and Fe II features are best modelled by the two highest redshift components only. Due to the blending between the components, we cannot directly determine the temperature of the gas reservoir. We therefore assume $T = 1 \times 10^4$ K (this is typical for metal-poor DLAs; see Cooke et al. 2015; Welsh et al. 2020; Noterdaeme et al. 2021). Given this assumed temperature, the associated turbulent broadening of these components are best described by the Doppler parameters $b_1 = 8.8 \pm 0.3$ km s^{-1}, $b_2 = 9.6 \pm 0.5$ km s^{-1}, and $b_3 = 14.9 \pm 0.7$ km s^{-1} respectively. The data, along with the best fitting model, are shown in Figure 1 while the resulting column densities and relative abundances are presented in Table 1. We note that, when modelling the the reported abundances, we allow the relative abundances of metals to vary from component to component. We have repeated our analysis under the assumption that the relative abundances of metals (i.e. the [O/Fe] ratio) must be constant across the components; the resulting total abundances are consistent with those reported in Table 1. In this metallicity regime, we do not expect our observed abundances to be impacted by any appreciable dust depletion (Pettini et al. 1997; Akerman et al. 2005; Vladilo et al. 2011; Rafelski et al. 2014).

The reported relative abundances are consistent with those found using the original HIRES data. Notably, we have improved the upper limit on the [Fe/H] abundance determination by ~ 1 dex from [Fe/H] < -2.81 (2σ) to [Fe/H] ≤ -3.66 (2σ). The DLA in question is therefore pushing towards the UMP regime at [Fe/H] < -4. Assuming these data are consistent with the typical [O/Fe] abundance of EMP DLAs reported in Welsh et al. (2022), the observed O I column density suggests that $[{\rm Fe/H}]_{\rm EMP} \simeq -3.72$. This predicted value is close to the reported upper limit. Additionally, we note that the reported [Fe/H] upper limit rules out the predicted [Fe/H] abundance given the typical [O/Fe] abundance of a very metal-poor (VMP; [Fe/H] < -2) DLA ($[{\rm Fe/H}]_{\rm VMP} \simeq -3.45$). During our analysis we have also placed the first upper limit on an odd-atomic number element, [Al/H] ≤ -3.76 (2σ). As will be discussed in subsequent sections, this is a useful indicator of the explosion mechanism of the enriching stellar population.

[5] We visually inspected the troughs of saturated absorption features to confirm this is the case.

These new data reaffirm that the DLA towards J0903+2628 is the most metal-poor DLA currently known. It has the lowest C, O, Si, and Fe abundance determination of any known DLA. We also searched for absorption from higher ion stages, such as Si III, so that we can determine the ionization ratio and subsequently model the density of the gas reservoir. However, the strong Si III λ1206 features is heavily blended with unrelated absorption. In the following sections, we investigate the chemical enrichment history of this DLA using our stochastic chemical enrichment model and the yields from simulations of Population III SNe.

3.1. *Chemical enrichment model*

Using the observed abundance pattern of this DLA, alongside the stochastic chemical enrichment model described in Welsh et al. (2019), we investigate the possible enrichment history of this DLA. The basis of our model is described below.

3.1.1. *Likelihood modelling technique*

The mass distribution of Population III stars is modelled as a power-law: $\xi(M) = k\,M^{-\alpha}$, where α is the power-law slope[6], and k is a multiplicative constant that is set by defining the number of stars, $N_\star$, that form between a minimum mass $M_{\rm min}$ and maximum mass $M_{\rm max}$, given by:

$$N_\star = \int_{M_{\rm min}}^{M_{\rm max}} k M^{-\alpha} dM \; . \tag{1}$$

In this work, $N_\star$ represents the number of stars that have contributed to the enrichment of a system. Since the first stars are thought to form in small multiples, this underlying mass distribution is necessarily stochastically sampled. We utilise the yields from simulations of stellar evolution to construct the expected distribution of chemical abundances given an underlying IMF model. These distributions can then be used to assess the likelihood of the observed DLA abundances given an enrichment model.

Specifically, the likelihood of a given enrichment model is calculated as the probability of the observed abundance pattern, R_o, given the abundance pattern expected from that enrichment model, R_m:

$$\mathcal{L} = p(R_o | R_m) \; . \tag{2}$$

In our analysis, we consider four abundance ratios. Therefore, for a given enrichment model, the probability of a system's chemical composition is given by the

[6] In our formulation, $\alpha = 2.35$ corresponds to a Salpeter IMF.

Table 1. Ion column densities of the DLA at $z_{\rm abs} = 3.07759$ towards the quasar J0903+2628. The quoted column density errors are the 1σ confidence limits while the column densities are given by $\log_{10} N({\rm X})/{\rm cm}^{-2}$.

Ion	Transitions used [Å]	Solar	Comp. 1 $z_{\rm abs} = 3.077589$	Comp. 2 $z_{\rm abs} = 3.076653$	Comp. 3 $z_{\rm abs} = 3.076331$	Total	[X/H]	[X/Fe]
H I	1215	12.00	—	—	—	20.32 ± 0.05	—	—
C II	1036, 1334	8.43	13.07 ± 0.03	12.99 ± 0.04	12.83 ± 0.06	13.45 ± 0.08	-3.42 ± 0.07	$> +0.24$
O I	988, 1302	8.69	13.70 ± 0.02	13.55 ± 0.03	—	13.93 ± 0.04	-3.08 ± 0.06	$> +0.58$
Al II	1670	6.45	≤ 9.78[a]	≤ 10.97[a]	—	≤ 11.00[a]	≤ -3.76[a]	—
Si II	1260, 1526	7.51	12.40 ± 0.01	12.20 ± 0.03	12.50 ± 0.02	12.86 ± 0.04	-3.22 ± 0.06	$> +0.44$
Fe II	1260, 1608, 2382	7.47	≤ 11.83[a]	≤ 11.83[a]	—	≤ 12.13[a]	≤ -3.66[a]	—

[a] 2σ upper limit on column density.

Total is given by sum of all available components, while abundance ratios consider only the first two components.

joint probability of these four abundance ratios. The probability of an observed abundance pattern is given by

$$p(R_o|R_m) = \int p(R_o|R_i)p(R_i|R_m){\rm d}R_i \, . \qquad (3)$$

The first term of this integral describes the probability of the observed abundance pattern being equal to the intrinsic abundance ratio of the system, R_i. For abundances with known errors, this distribution is modelled by a Gaussian. For abundances with upper limits, this distribution is modelled by a Q-function. The second term of the integral in Equation 3 describes the probability of obtaining an intrinsic abundance pattern given the IMF defined in Equation 1. We utilise the yields from Heger & Woosley (2010) (hereafter HW10) to construct the expected distribution of chemical abundances given an underlying IMF model.

The HW10 simulations trace nucleosynthesis processes within Population III progenitors across their lifetimes and calculate the ejected yields of elements following the eventual collapse of these stars as core-collapse SNe (CCSNe). These simulations explore initial progenitor masses that span from $M = (10 - 100)$ M$_\odot$, explosion energies from $E_{\rm exp} = (0.3 - 10) \times 10^{51}$ erg, and mixing parameters from $f_{\rm He} = 0 - 0.25$. The explosion energy is a measure of the final kinetic energy of the ejecta at infinity, while the mixing between stellar layers is parameterised as a fraction of the helium core size. This parameter space is evaluated across 120 masses, 10 explosion energies, and 14 mixing parameters. We linearly interpolate between this grid of yields during our analysis. We refer the reader to HW10 and Welsh et al. (2019) for further details and caveats related to these yield calculations.

Our model contains six parameters: $N_\star$, α, $M_{\rm min}$, $M_{\rm max}$, $E_{\rm exp}$ and $f_{\rm He}$. The range of model parameters we consider are:

$$\begin{aligned} -5 \leq \quad & \alpha \quad & \leq 5 \, , \\ 1 \leq \quad & N_\star \quad & \leq 150 \, , \\ 0.3 \leq \, & E_{\rm exp}/10^{51}{\rm erg} & \leq 10 \, , \\ 12 \leq \, & M_{\rm max}/{\rm M}_\odot & \leq 70 \, . \end{aligned}$$

In what follows, we assume that stars with masses > 10 M$_\odot$ are physically capable of undergoing core-collapse. Therefore, we fix $M_{\rm min} = 10$ M$_\odot$. We also assume that the mixing during the explosive burning phase of the SN occurs within a region 10 per cent of the helium core size (i.e. $f_{\rm He} = 0.100$). This is the fiducial choice from the HW10 based on their comparison with the Cayrel et al. (2004) stellar sample. We apply uniform priors to all remaining model parameters. Note that the upper bound on $M_{\rm max}$ corresponds to the mass limit above which pulsational pair-instability SNe are believed to occur (Woosley 2017).

3.2. *Application to DLA data*

Using all available chemical abundance measurements of the DLA towards J0903+2628 we run a Markov Chain Monte Carlo (MCMC) maximum likelihood analysis to find the enrichment model that best fits these data. The converged chains are shown in Figure 2 for both a Salpeter IMF (green histograms and contours) and a free IMF slope (grey histograms and contours). The inferred enrichment models are broadly consistent for both the choice of a varying and fixed IMF slope. This is to be expected since the maximum likelihood estimate of α for the varying IMF slope is consistent with that of a Salpeter distribution at the 95 per cent confidence level. However, we note there is preference towards a flat or even top-heavy IMF slope. The inferred number of enriching stars shows a preference towards low values of $N_\star$. The distribution of the typical explosion energy is more clearly centred around $E_{\rm exp} \sim 1.8 \times 10^{51}$ erg. Both the distribution of $N_\star$ and $E_{\rm exp}$ are stable against changes to the slope of the IMF. In contrast to this, the inferred maximum mass of the enriching star is depen-

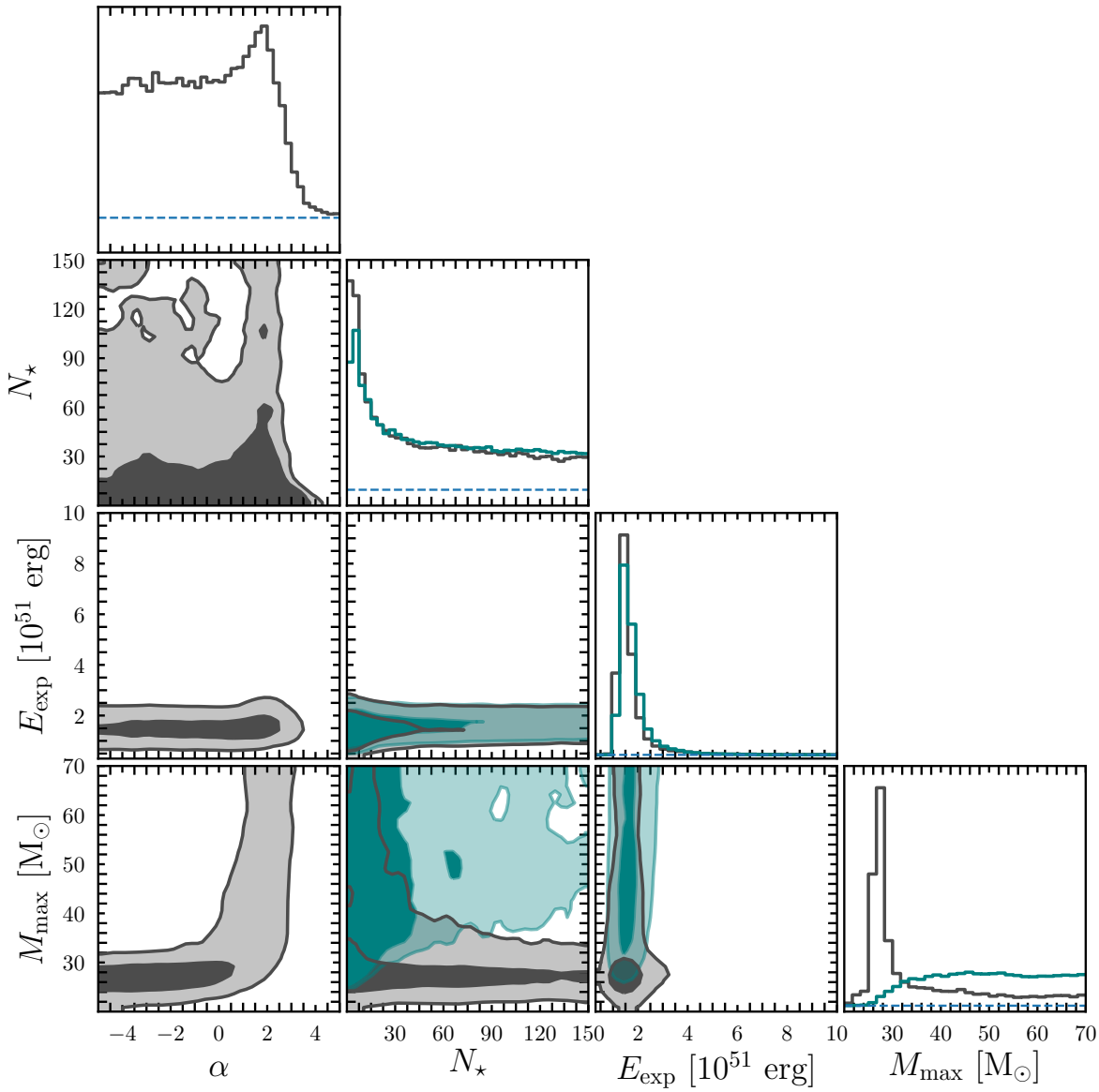

Figure 2. The marginalised maximum likelihood distributions of our fiducial model parameters (main diagonal), and their associated 2D projections, given the known chemistry of the DLA towards J0903+2628. The dark and light contours show the 68% and 95% confidence regions of these projections respectively. The horizontal blue dashed lines mark where the individual parameter likelihood distributions fall to zero. The grey distributions correspond to the analysis of the full parameter space, described in Section 3.1. The green distributions are the result of imposing a Salpeter slope for the IMF (i.e. $\alpha = 2.35$).

dent on the slope of the IMF. For a Salpeter distribution, there is preference towards $M_{\rm max} > 40$ M$_\odot$; this can be seen from the plateau in the distribution shown in the bottom right panel of Figure 2. For the case of a varying IMF slope, there is a peak in the distribution of the maximum mass at $M_{\rm max} \sim 25$ M$_\odot$. This is driven by the possibility of both flat and top-heavy IMFs. This can be seen by the correlation between α and $M_{\rm max}$ in the bottom left panel of Figure 2. These results are consistent with our previous investigations of the enrichment of metal-poor DLAs.

The broad distributions in Figure 2 highlight the lack of preference towards a particular enrichment model (e.g. both the number of enriching stars and the maximum stellar mass are relatively unconstrained). To investigate the origin of this, we test how well the inferred model can replicate the data. Using our stochastic enrichment model, we can recover the predicted abundance pattern given the inferred parameter distributions. The

modelled abundances are shown alongside the observational measurements (red symbols) in Figure 3 for the case of a free IMF slope (blue symbols) and for a Salpeter IMF slope (orange symbols). While the observed abundance pattern is well-recovered, there is a preference towards a top-heavy IMF and a low number of enriching stars. The predicted abundances given a Salpeter IMF do not produce the same agreement with the observed abundances of the DLA. For this reason, we now consider the possibility that this system has been enriched by a single Population III SN.

The results of this analysis are shown in Figure 4. Note that, in this scenario, we allow the degree of mixing to vary as a free parameter with a uniform prior. Figure 4 highlights that there is a clear peak in the distribution of the inferred initial progenitor mass. The peak is well centred between $M = (25 - 30)\mathrm{M}_{\odot}$ corresponds to a progenitor with a low explosion energy, described by $E_{\mathrm{exp}} = (0.3 - 3) \times 10^{51}$ erg (1σ). This progenitor shows a preference towards and high degree of mixing between the stellar layers, $f_{\mathrm{He}} > 0.1$ (1σ), though it is unconstrained at a 2σ level. The lack of information regarding the degree of mixing is curious — it may be related to the increased variability of the predicted yields (across small mass scales) that is introduced when varying this parameter.

In Figure 3, we show the modelled abundance ratios given the distributions of progenitor parameters shown in Figure 4. From this figure, it is clear that the scenario of enrichment by an individual Population III SN is a similarly good model fit to the data as the stochastic model shown in Figure 2. This can be seen through the comparison of the left and hand panels of Figures 3. The predicted abundances in the both scenario are likely being drawn from similar progenitors. The maximum likelihood parameter estimates from the stochastic model are consistent with a sampling an individual ~ 25 $\mathrm{M}_{\odot}$ progenitor (achieved via a top-heavy IMF model with $N_{\star} = 1$ and $M_{\mathrm{max}} = 25$ $\mathrm{M}_{\odot}$). The observed upper limits of [Fe/O] are more easily explained given the yields of an individual Population III SN. Though, the true level of agreement is reserved for a definitive [Fe/O] measurement. It is interesting that the known abundances of this DLA are preferably modelled by the yields of an individual Population III SN rather than a small handful of these progenitors. We have also repeated our analysis under the assumption of enrichment by an individual Population II star and found that, using the yields from Woosley & Weaver (1995), the enrichment by a Population III star is preferable (see Appendix for further details). The case of enrichment by an individual Population III SN is often reserved for the stellar relics found in the halo of the Milky Way and surrounding dwarf galaxies. In the following section, we discuss the implications of these results and draw comparisons with the chemistry of other relic objects. Ultimately, the goal is to reveal the nature of this most metal-poor DLA and its place within galaxy evolution.

4. DISCUSSION

The nature of DLAs, especially the most metal-poor systems, is still an open question. One possibility, that has been discussed since the first DLA survey, is that these highest column density absorption line systems are associated with the discs of high redshift galaxies (Wolfe et al. 1986). Searches for the emission from host galaxies aim to illuminate this issue. The use of integral field spectrographs have proven to be fruitful tools for these searches (e.g. Péroux et al. 2011, 2012; Fumagalli et al. 2017; Mackenzie et al. 2019; Berg et al. 2022; Lofthouse et al. 2022); as has the Atacama Large Millimeter/submillimeter Array (ALMA) (e.g. Møller et al. 2018; Neeleman et al. 2018; Klitsch et al. 2021). Surveys with these instruments may tentatively indicate that there is a more complicated relationship between the column density of the absorbing gas and its association with the host galaxy than initially thought (e.g. Lofthouse et al. 2022).

Specifically considering DLAs, the majority of searches have led to non-detections of host galaxies (e.g. Kulkarni et al. 2000; Fynbo et al. 2010; Fumagalli et al. 2015; Møller et al. 2018; Ranjan et al. 2020). It is unclear whether this low detection rate is due to observational challenges or whether it is an indication of the fraction of the population associated with active star formation. A review of observational efforts suggests there may be a steep relationship between the emission luminosity of the host galaxy and the metallicity of the DLA (Krogager et al. 2017). There is yet to be a detection in emission of a host galaxy associated with one of the four known EMP DLAs. Consequently, we look to other means to understand the association between the most metal-poor DLAs and galaxy evolution.

The chemistry of these environments is an invaluable tool to link these gaseous relics seen at high redshift to their local descendants. This is a necessary step to understand the role of near-pristine DLAs in galaxy evolution. Furthermore, it facilitates comparisons with other relic environments that may reveal similar enrichment histories and shared evolutionary pathways. For this reason, the following section is dedicated to comparing the chemistry of the most metal-poor DLA known to the stars within ultra-faint dwarf galaxies (UFDs).

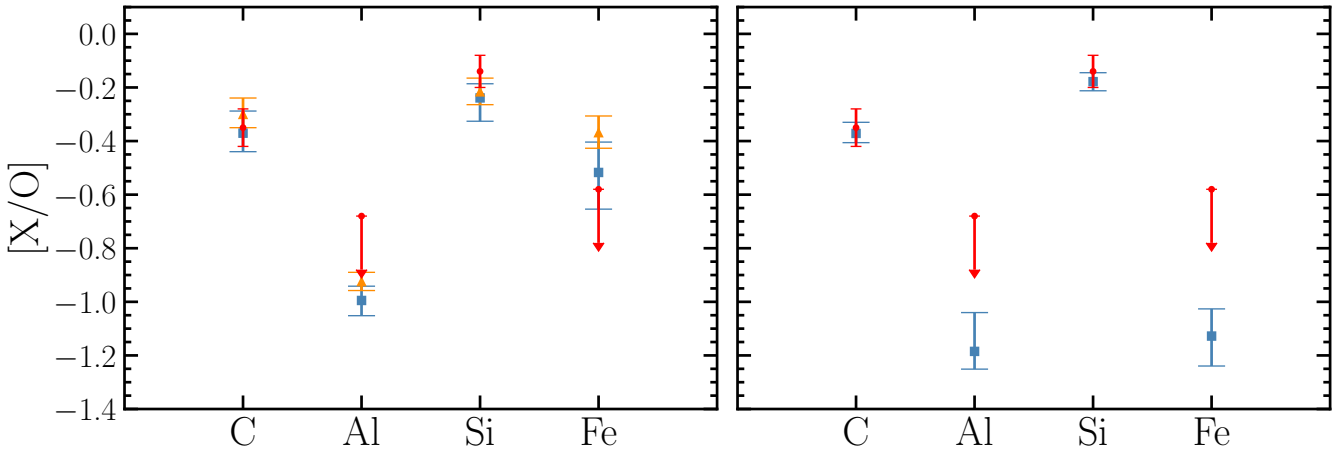

Figure 3. Left: Modelled abundances (blue) vs. observed data (red) given a stochastic enrichment model with a free IMF slope. The model successfully reproduces all chemical abundance measurements. The blue data show the median predicted value and the associated errors encompass the interquartile range. For reference the modelled abundances given a Salpeter IMF are shown in orange. Right: Modelled abundances (blue) vs. observed data (red) under the assumption that the environment has been enriched by 1 SN.

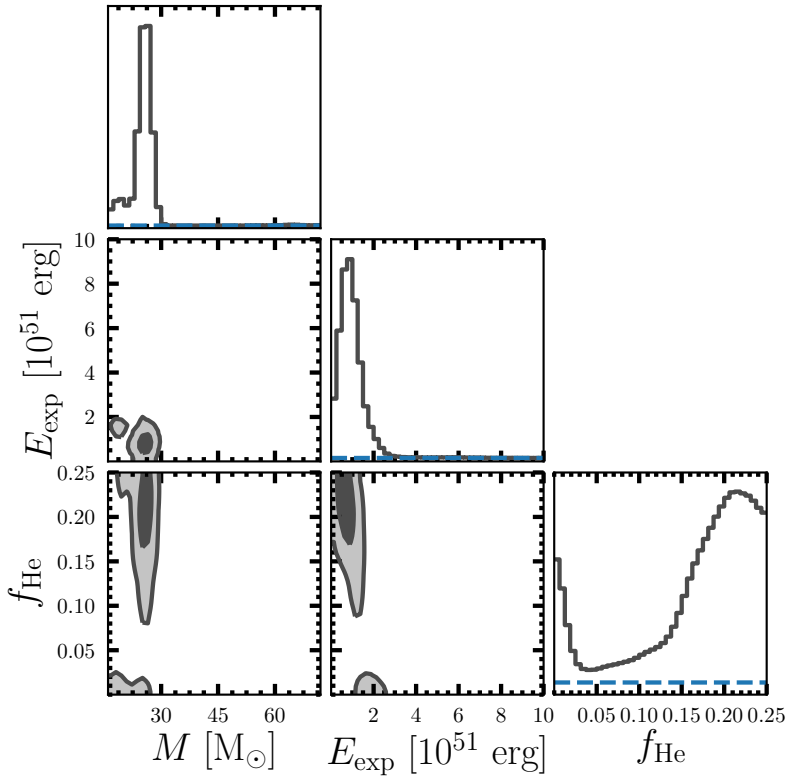

Figure 4. Results of our MCMC analysis of the chemical enrichment of the DLA towards J0903+2628 assuming the number of enriching stars $N_\star = 1$. From left to right, we show the progenitor star mass, the explosion energy, and the degree of mixing. The diagonal panels indicate the maximum likelihood posterior distributions of the model parameters while the 2D contours indicate the correlation between these parameters. The dark and light gray shaded regions indicate the 68 and 95 per cent confidence intervals, respectively. In the diagonal panels, the horizontal blue dashed line indicates the zero-level of each distribution.

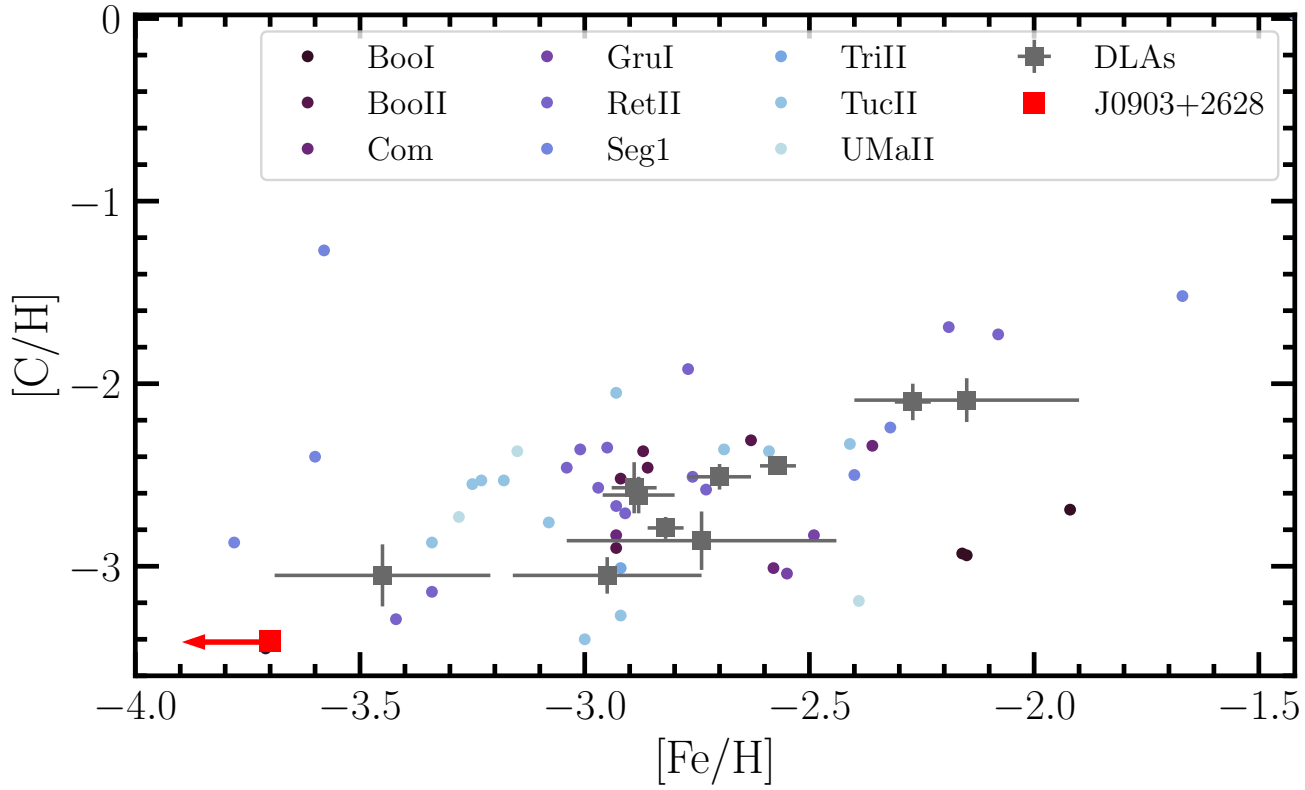

Figure 5. [C/H] vs [Fe/H] abundances of stars in ultra faint dwarf galaxies alongside that of the most metal-poor DLAs. Stellar data is from the SAGA database and includes: Bootes I, Bootes II, Canes Venatici II, Coma Berenices, Grus I, Grus II, Leo IV, Leo V, Pisces II, Tucana II, Tucana III, Ursa Major, and Willman I. These are distinguished by their colour as described in the legend. The abundances reported here are shown by the red square.

4.1. *Comparison with UFDs*

We now compare the chemistry of this DLA to the chemistry of stars in the ultra faint dwarf galaxies (UFDs; $M_V > -7.7$ from the definition by Simon (2019)) that orbit the Milky Way. The lowest mean metallicity of a confirmed UFD is that of Tucana II with [Fe/H] $= -2.9^{+0.15}_{-0.16}$ (Bechtol et al. 2015; Walker et al. 2016; Chiti et al. 2018; Simon 2019). These ancient galaxies are on the borderline of extreme metal-paucity and are considered relics of the early Universe (Salvadori & Ferrara 2009; Bovill & Ricotti 2009; Muñoz et al. 2009; Bromm & Yoshida 2011).

There are five stars within UFDs with Fe-metallicities lower than our reported upper limit. From these, there is only one with an associated error less than 5 per cent. This is SDSS J10063933+1600086 commonly known as Seg 1 161 (Simon et al. 2011). The star in question has a reported [CH/Fe] $= +0.91 \pm 0.25$, [Si/Fe] $= +1.27 \pm 0.25$, and [Fe/H] $= -3.78 \pm 0.11$ (Frebel et al. 2014). Thus, while the Fe-metallicity is low, the entire chemistry of this system is not as metal deficient as the DLA reported here.

To perfectly compare the metallicity of the DLA towards J0903+2628 with similar stellar relics would require the detection of the same elements across each system. Given that a larger range of elements are observable for stellar relics, in addition to the different physics required to model each environment, this is not typically possible. We therefore reserve our analysis to comparing the relative abundance of an α-element (in this case [C/H]) alongside that of [Fe/H]. Figure 5 shows [C/H] as a function of [Fe/H] for both metal-poor DLAs (grey squares) and stars within UFDs (color-coded circles). The system reported here is shown as the red square. From this plot, we can see that the DLA reported here is one of the most Fe-poor objects known that is not overabundant in C.

Interestingly, there is an EMP star within Boötes I (purple circle in Figure 5) that occupies a similar parameter space as the DLA reported here. This star is known as Boo-1137. The relative abundances of mutual elements (i.e. those also detected towards J0903+2628) are provided in Table 2. These are taken from Norris et al. (2010) who use the solar scale log $\epsilon_{Fe} = 7.45$[7].

[7] log $\epsilon_X \equiv$ log(X/H) + 12. This is from Asplund (2005). Note, we adopt the solar scale referenced in Table 1. In more recent stellar studies it is typical to assume log $\epsilon_{Fe} = 7.51$. This, like our solar scale, is drawn from Asplund et al. (2009). On the solar scale typically used in stellar studies, our Fe limit would be [Fe/H] < -3.70 (2σ).

Table 2. Elemental abundance ratios of Boo-1137 from Norris et al. (2010), corrected to the solar abundance scale adopted in our work. The quoted errors are the 1σ confidence limits while the upper limits are 2σ.

El	$[X/H]_{DLA}$	$[X/H]_\star$
C	-3.42 ± 0.07	-3.45 ± 0.20
O	-3.08 ± 0.06	< -1.75
Al	≤ -3.76	-4.35 ± 0.11
Si	-3.22 ± 0.06	-2.89 ± 0.16[a]
Fe	≤ -3.66	-3.68 ± 0.11

[a] This error given by that of [Si/Fe] which is the ratio used in the MCMC enrichment model analysis.

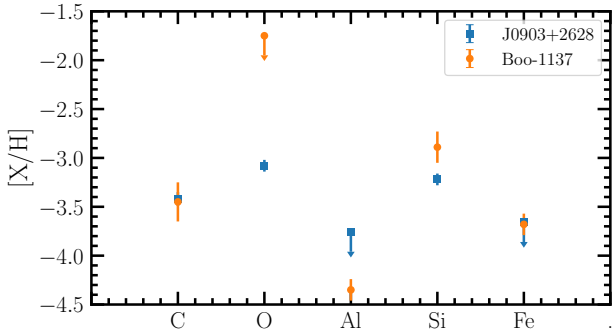

Figure 6. Comparisons of the [X/H] abundances of the common chemical elements detected for J0903+2628 (blue) and Boo−1137 (orange).

After rescaling the [Fe/H] abundance to the solar value provided in Table 1, Figure 6 visualises this comparison of similar relative abundances. While the upper limits provide limited information, the abundances of these environments appear to be consistent. We speculate that this common chemical abundance pattern may indicate a common formation channel. In other words, the similar chemistry of these environments may imply they were enriched by a similar (possibly primordial) population of stars. Repeating our MCMC analysis, under the assumption of enrichment from 1 Population III SN, on Boo−1137 converges on progenitor properties similar to those found for J0903+2628. During this analysis, we utilised the same chemical elements used for J0903+2628. Though, to accommodate the upper limit on [O/H], we consider the abundance ratios relative to Fe instead of O. The results of this analysis and the corresponding fit to the data can be are shown Figures 7 and 8 respectively. We do not take the analysis further as our best fit progenitor for Boo−1137 struggles to replicate the observed [Si/Fe] ratio alongside the other elements. Note that we considered a combination

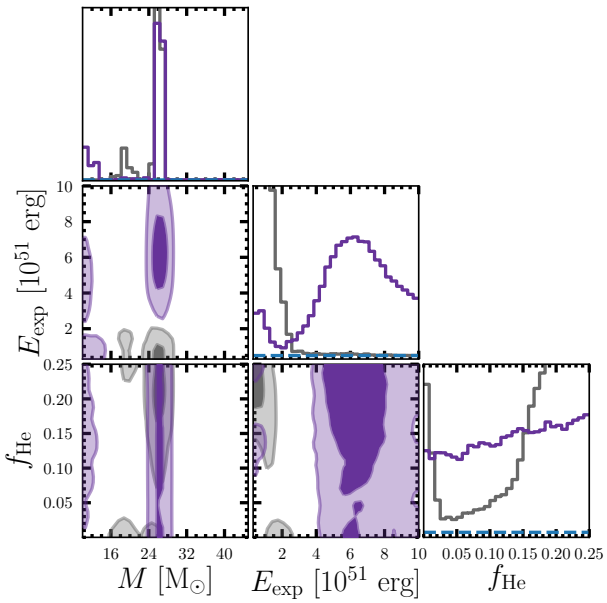

Figure 7. Same as Figure 4 for given [C/Fe], [Si/Fe], [O/Fe], and [Al/Fe] of Boo−1137. The distributions associated with Boo−1137 are shown in purple while those for J0903+2628 (from Figure 4) are shown in grey for reference.

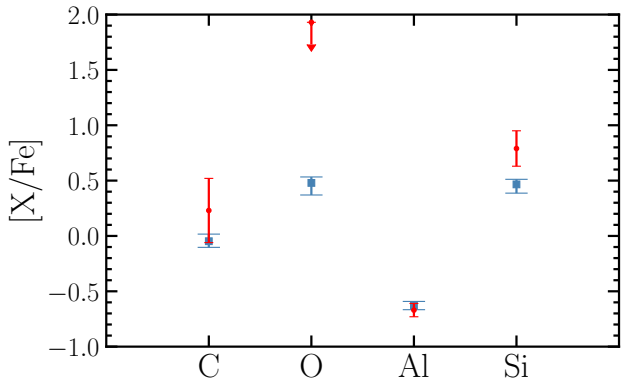

Figure 8. Same as Figure 3 for enrichment model inferred for Boo−1137

of different abundance ratios in our analysis and found a similar result.

Ultimately, despite the broadly similar abundances, these relics are only somewhat well-modelled by a common progenitor given our analysis. A more striking agreement between the inferred progenitor properties is needed to provide a compelling argument for a shared enrichment channel. We are currently limited by the information provided from the observed upper limits.

As things stand, we need more information to link the most metal-poor DLA currently known to its local analogues. This information can be gained in a multitude of ways. First, as previously mentioned, NIR observations will allow a determination of the Fe column density through the Fe II λ2382 feature. Furthermore, within the next decade, we will see the advent of the next generations of $\sim$ 30+ m optical/IR ground-based telescopes, including the Extremely Large Telescope (ELT; Gilmozzi & Spyromilio 2007), the Giant Magellan Telescope (GMT; Johns et al. 2012), and the Thirty Meter Telescope (TMT; Skidmore et al. 2015). With these facilities we will be able to study the *most* metal-poor DLAs with unprecedented sensitivity. Thus, we will be able to determine the abundances of elements whose features are too weak to efficiently determine with current facilities (e.g. the N, Mg, S, Al, Fe, Ni, Zn, and Cr of J0903+2628). Beyond chemistry, we can use additional diagnostics (e.g. kinematics, density models, host galaxy emission, environment etc.) to investigate the properties of these ancient relics and their surrounding galaxy populations.

4.2. *Observations with JWST*

With the JWST, it may be possible to detect light directly from the first stars at high redshift. However, depending on the adopted formation formalism, it may be infeasible to detect light from the first stellar population at $z > 8$ without the aide of lensing (Bovill et al. (2022); see also Trussler et al. (2022) for a more optimistic outlook).

The most metal-poor DLAs, and indeed near-pristine systems with lower column densities, provide a signpost to some of the least chemically polluted environments at $z_{\rm abs} < 6$. Such environments might be ideal to conduct searches for Population III stars at lower, more accessible, redshifts. Depending on the redshift of the absorber (e.g. $3 < z_{\rm abs} < 6$), the strong He II λ1640 Å feature expected from Population III stars may be most efficiently studied from the ground (using an optical IFU) or from space (with HST/WFC3 or JWST/NIRCam). Once the strong He II λ1640 Å emission has been identified, JWST/NIRSpec is the optimal instrument to confirm the Population III nature of this emission by searching for strong H Balmer emission lines (indicative of an H II region), combined with the absence of associated metal emission (e.g. [O III] λ 5007Å). Given the challenges associated with detecting Population III stars at $z > 8$, the most metal-poor DLAs may be invaluable tools in the search for light from the first stars. Over the coming years, observational surveys are necessary to explore how efficient these DLAs are as beacons for the first stars and galaxies. Furthermore, the firm detection of a Population III stellar signature associated with

these DLA host galaxies would confirm the relic nature of these environments.

5. CONCLUSIONS

We present the updated chemical abundances of the the DLA towards J0903+2628 based on data collected with Keck I/HIRES. These data reaffirm that this gas reservoirs is the most metal-poor DLA currently known. Our main conclusions are as follows:

1. The latest data provide an upper limit on the iron abundance, [Fe/H]≤ -3.66 (2σ). This is a 0.85 dex improvement on the previous upper limit and confirms that this DLA is indeed EMP, and could possibly be the first UMP DLA. To secure the first firm detection of Fe in this system will require further observations. This would require a significant time investment on $8-10$ m class telescopes. Alternatively, the required sensitivity will be efficiently achieved with the next generation of $30-40$ m telescopes.

2. The current data indicate that *all* of the detected $\alpha-$elements (C, O, and Si) are enhanced relative to iron, compared to a typical very metal-poor DLA. We speculate that this intriguing gas cloud may have an iron abundance considerably below the current detection limit. Such an Fe-deficient abundance pattern is reminiscent of the α-enhanced (or, rather, Fe-deficient) stars in the halo of the Milky Way.

3. We apply a stochastic chemical enrichment model to investigate the properties of the stars that have enriched this gaseous relic. The results of this analysis suggest that the chemistry of this environment is best modelled by a low number of enriching stars. The observed abundance pattern is best fit by an individual Population III SN with an initial progenitor mass that was $M = (25-30)\mathrm{M}_{\odot}$ (2σ).

4. We compare the chemistry of this DLA to the abundances of the most metal-poor stars in the UFDs orbiting the Milky Way. The star closest in chemistry to that of the DLA towards J0903+2628 is Boo$-$1137 in Boötes I with [Fe/H] $= -3.68\pm0.11$ (registered onto our adopted solar scale; Norris et al. 2010). Comparing the [X/H] abundances of common elements across these relics shows a broadly consistent chemistry. This may indicate that Boo$-$1137 formed from gas that was enriched by a similar mass (possibly Pop. III) star that was responsible for the enrichment of J0903+2628. Indeed, our analysis tentatively supports the scenario in which these relics have been enriched by an single Population III progenitor with similar properties.

Our work highlights that, while rare, these near-pristine DLAs are an invaluable probe of the metals produced by some of the earliest stars in the Universe. These gaseous relics may also provide a signpost to some of the least polluted environments of the Universe and thus act as beacons to search for light from the first stars directly using JWST.

This paper is based on observations collected at the W. M. Keck Observatory which is operated as a scientific partnership among the California Institute of Technology, the University of California and the National Aeronautics and Space Administration. The Observatory was made possible by the generous financial support of the W. M. Keck Foundation. The authors wish to recognize and acknowledge the very significant cultural role and reverence that the summit of Maunakea has always had within the indigenous Hawaiian community. We are most fortunate to have the opportunity to conduct observations from this mountain. We are also grateful to the staff astronomers at Keck Observatory for their assistance with the observations. This work has been supported by Fondazione Cariplo, grant No 2018-2329. During this work, R. J. C. was supported by a Royal Society University Research Fellowship. We acknowledge support from STFC (ST/L00075X/1, ST/P000541/1). This project has received funding from the European Research Council (ERC) under the European Union's Horizon 2020 research and innovation programme (grant agreement No 757535). This work used the DiRAC Data Centric system at Durham University, operated by the Institute for Computational Cosmology on behalf of the STFC DiRAC HPC Facility (www.dirac.ac.uk). This equipment was funded by BIS National E-infrastructure capital grant ST/K00042X/1, STFC capital grant ST/H008519/1, and STFC DiRAC Operations grant ST/K003267/1 and Durham University. DiRAC is part of the National E-Infrastructure. This research has made use of NASA's Astrophysics Data System.

Facilities: Keck:I (HIRES)

Software: Astropy (Astropy Collaboration et al. 2013), Corner (Foreman-Mackey 2016), Matplotlib (Hunter 2007), and NumPy (van der Walt et al. 2011).

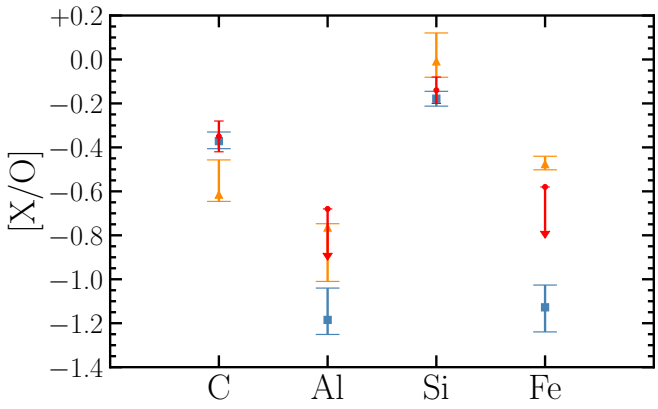

Figure 9. Same as Figure 3 for enrichment model inferred for a Population II progenitor (orange) alongside those inferred for a Population III progenitor (blue).

APPENDIX

A. ENRICHMENT BY POPULATION II STARS

In this appendix we repeat our MCMC analysis to find the properties of 1 Population II SN that best match the abundances of the DLA reported here. For this analysis we utilise a subset of the yields from Woosley & Weaver (1995) whose progenitor metallicities are $Z = 0.0001 Z_{\odot}$. These yields span a mass range of $M = (12-40)$ $M_{\odot}$; this is the same region explored during our analysis. The yields are calculated using a fixed explosion energy and mixing parameter therefore the only free parameter in this analysis is the progenitor mass. We find the yields are best modelled by a star will a mass $M \sim 27$ $M_{\odot}$. The relative abundances estimated given the inferred parameter distribution is shown in Figure 9 alongside the observed abundances and those predicted from our analysis using Population III yields. From this figure, we can see that the Population III star abundances (blue) are a better fit to the data than the Population II star abundances (orange). A caveat to note is that the Population II yields are comparatively limited given the fixed explosion energy and mixing parameter adopted during the Woosley & Weaver (1995) simulations. However, given the available yields, a Population III progenitor is better able to replicate the observed relative abundances.

REFERENCES

Abel, T., Bryan, G. L., & Norman, M. L. 2002, Science, 295, 93, doi: 10.1126/science.295.5552.93

Akerman, C. J., Ellison, S. L., Pettini, M., & Steidel, C. C. 2005, A&A, 440, 499, doi: 10.1051/0004-6361:20052947

Asplund, M. 2005, ARA&A, 43, 481, doi: 10.1146/annurev.astro.42.053102.134001

Asplund, M., Grevesse, N., Sauval, A. J., & Scott, P. 2009, ARA&A, 47, 481, doi: 10.1146/annurev.astro.46.060407.145222

Astropy Collaboration, Robitaille, T. P., Tollerud, E. J., et al. 2013, A&A, 558, A33, doi: 10.1051/0004-6361/201322068

Bañados, E., Rauch, M., Decarli, R., et al. 2019, ApJ, 885, 59, doi: 10.3847/1538-4357/ab4129

Barkana, R., & Loeb, A. 2001, PhR, 349, 125, doi: 10.1016/S0370-1573(01)00019-9

Bechtol, K., Drlica-Wagner, A., Balbinot, E., et al. 2015, ApJ, 807, 50, doi: 10.1088/0004-637X/807/1/50

Becker, G. D., Sargent, W. L. W., Rauch, M., & Calverley, A. P. 2011, ApJ, 735, 93, doi: 10.1088/0004-637X/735/2/93

Becker, G. D., Pettini, M., Rafelski, M., et al. 2019, ApJ, 883, 163, doi: 10.3847/1538-4357/ab3eb5

Beers, T. C., & Carollo, D. 2008, in American Institute of Physics Conference Series, Vol. 990, First Stars III, ed. B. W. O'Shea & A. Heger, 104–108, doi: 10.1063/1.2905513

Beers, T. C., & Christlieb, N. 2005, ARA&A, 43, 531, doi: 10.1146/annurev.astro.42.053102.134057

Beers, T. C., Preston, G. W., & Shectman, S. A. 1985, AJ, 90, 2089, doi: 10.1086/113917

—. 1992, AJ, 103, 1987, doi: 10.1086/116207

Berg, M. A., Lehner, N., Howk, J. C., et al. 2022, arXiv e-prints, arXiv:2204.13229. https://arxiv.org/abs/2204.13229

Bond, H. E. 1980, The Astrophysical Journal Supplement Series, 44, 517, doi: 10.1086/190703

Bosman, S. E. I., & Becker, G. D. 2015, MNRAS, 452, 1105, doi: 10.1093/mnras/stv1336

Bosman, S. E. I., Davies, F. B., Becker, G. D., et al. 2022, MNRAS, 514, 55, doi: 10.1093/mnras/stac1046

Bovill, M. S., & Ricotti, M. 2009, ApJ, 693, 1859, doi: 10.1088/0004-637X/693/2/1859

Bovill, M. S., Stiavelli, M., Wiggins, A. I., Ricotti, M., & Trenti, M. 2022, arXiv e-prints, arXiv:2210.10190. https://arxiv.org/abs/2210.10190

Bromm, V., Coppi, P. S., & Larson, R. B. 2002, ApJ, 564, 23, doi: 10.1086/323947

Bromm, V., & Yoshida, N. 2011, ARA&A, 49, 373, doi: 10.1146/annurev-astro-081710-102608

Cayrel, R., Depagne, E., Spite, M., et al. 2004, A&A, 416, 1117, doi: 10.1051/0004-6361:20034074

Chiti, A., Frebel, A., Ji, A. P., et al. 2018, ApJ, 857, 74, doi: 10.3847/1538-4357/aab4fc

Christlieb, N., Schörck, T., Frebel, A., et al. 2008, A&A, 484, 721, doi: 10.1051/0004-6361:20078748

Clark, P. C., Glover, S. C. O., Klessen, R. S., & Bromm, V. 2011, ApJ, 727, 110, doi: 10.1088/0004-637X/727/2/110

Cooke, R., Pettini, M., Steidel, C. C., Rudie, G. C., & Jorgenson, R. A. 2011a, MNRAS, 412, 1047, doi: 10.1111/j.1365-2966.2010.17966.x

Cooke, R., Pettini, M., Steidel, C. C., Rudie, G. C., & Nissen, P. E. 2011b, MNRAS, 417, 1534, doi: 10.1111/j.1365-2966.2011.19365.x

Cooke, R. J., Pettini, M., & Jorgenson, R. A. 2015, ApJ, 800, 12, doi: 10.1088/0004-637X/800/1/12

Cooke, R. J., Pettini, M., Nollett, K. M., & Jorgenson, R. 2016, ApJ, 830, 148, doi: 10.3847/0004-637X/830/2/148

Cooke, R. J., Pettini, M., & Steidel, C. C. 2017, MNRAS, 467, 802, doi: 10.1093/mnras/stx037

Dalton, G., Trager, S. C., Abrams, D. C., et al. 2012, in Society of Photo-Optical Instrumentation Engineers (SPIE) Conference Series, Vol. 8446, Ground-based and Airborne Instrumentation for Astronomy IV, ed. I. S. McLean, S. K. Ramsay, & H. Takami, 84460P, doi: 10.1117/12.925950

de Jong, R. S., Bellido-Tirado, O., Chiappini, C., et al. 2012, in Society of Photo-Optical Instrumentation Engineers (SPIE) Conference Series, Vol. 8446, Ground-based and Airborne Instrumentation for Astronomy IV, ed. I. S. McLean, S. K. Ramsay, & H. Takami, 84460T, doi: 10.1117/12.926239

DESI Collaboration, Aghamousa, A., Aguilar, J., et al. 2016, arXiv e-prints, arXiv:1611.00036. https://arxiv.org/abs/1611.00036

D'Odorico, V., Finlator, K., Cristiani, S., et al. 2022, MNRAS, 512, 2389, doi: 10.1093/mnras/stac545

Ellison, S. L., Prochaska, J. X., Hennawi, J., et al. 2010, MNRAS, 406, 1435, doi: 10.1111/j.1365-2966.2010.16780.x

Erni, P., Richter, P., Ledoux, C., & Petitjean, P. 2006, A&A, 451, 19, doi: 10.1051/0004-6361:20054328

Foreman-Mackey, D. 2016, The Journal of Open Source Software, 1, 24, doi: 10.21105/joss.00024

Frebel, A., Simon, J. D., & Kirby, E. N. 2014, ApJ, 786, 74, doi: 10.1088/0004-637X/786/1/74

Fumagalli, M., O'Meara, J. M., & Prochaska, J. X. 2011, Science, 334, 1245, doi: 10.1126/science.1213581

Fumagalli, M., O'Meara, J. M., Prochaska, J. X., Rafelski, M., & Kanekar, N. 2015, MNRAS, 446, 3178, doi: 10.1093/mnras/stu2325

Fumagalli, M., Mackenzie, R., Trayford, J., et al. 2017, MNRAS, 471, 3686, doi: 10.1093/mnras/stx1896

Fynbo, J. P. U., Laursen, P., Ledoux, C., et al. 2010, MNRAS, 408, 2128, doi: 10.1111/j.1365-2966.2010.17294.x

Gardner, J. P., Mather, J. C., Clampin, M., et al. 2009, in Astrophysics and Space Science Proceedings, Vol. 10, Astrophysics in the Next Decade, 1, doi: 10.1007/978-1-4020-9457-6_1

Gilmozzi, R., & Spyromilio, J. 2007, The Messenger, 127, 11

Greif, T. H., Glover, S. C. O., Bromm, V., & Klessen, R. S. 2010, ApJ, 716, 510, doi: 10.1088/0004-637X/716/1/510

Hartwig, T., Bromm, V., Klessen, R. S., & Glover, S. C. O. 2015, MNRAS, 447, 3892, doi: 10.1093/mnras/stu2740

Heger, A., & Woosley, S. E. 2010, ApJ, 724, 341, doi: 10.1088/0004-637X/724/1/341

Hirano, S., Hosokawa, T., Yoshida, N., et al. 2014, ApJ, 781, 60, doi: 10.1088/0004-637X/781/2/60

Howes, L. M., Asplund, M., Keller, S. C., et al. 2016, MNRAS, 460, 884, doi: 10.1093/mnras/stw1004

Hunter, J. D. 2007, Computing in Science and Engineering, 9, 90, doi: 10.1109/MCSE.2007.55

Johns, M., McCarthy, P., Raybould, K., et al. 2012, in Society of Photo-Optical Instrumentation Engineers (SPIE) Conference Series, Vol. 8444, Ground-based and Airborne Telescopes IV, ed. L. M. Stepp, R. Gilmozzi, & H. J. Hall, 84441H, doi: 10.1117/12.926716

Klitsch, A., Péroux, C., Zwaan, M. A., et al. 2021, MNRAS, 506, 514, doi: 10.1093/mnras/stab1668

Krogager, J. K., Møller, P., Fynbo, J. P. U., & Noterdaeme, P. 2017, MNRAS, 469, 2959, doi: 10.1093/mnras/stx1011

Kulkarni, V. P., Hill, J. M., Schneider, G., et al. 2000, ApJ, 536, 36, doi: 10.1086/308904

Lofthouse, E. K., Fumagalli, M., Fossati, M., et al. 2022, MNRAS, doi: 10.1093/mnras/stac3089

Mackenzie, R., Fumagalli, M., Theuns, T., et al. 2019, MNRAS, 487, 5070, doi: 10.1093/mnras/stz1501

McWilliam, A., Preston, G. W., Sneden, C., & Shectman, S. 1995, AJ, 109, 2736, doi: 10.1086/117485

Møller, P., Christensen, L., Zwaan, M. A., et al. 2018, MNRAS, 474, 4039, doi: 10.1093/mnras/stx2845

Muñoz, J. A., Madau, P., Loeb, A., & Diemand, J. 2009, MNRAS, 400, 1593, doi: 10.1111/j.1365-2966.2009.15562.x

Neeleman, M., Kanekar, N., Prochaska, J. X., et al. 2018, ApJl, 856, L12, doi: 10.3847/2041-8213/aab5b1

Norris, J. E., Yong, D., Gilmore, G., & Wyse, R. F. G. 2010, ApJ, 711, 350, doi: 10.1088/0004-637X/711/1/350

Noterdaeme, P., Balashev, S., Ledoux, C., et al. 2021, arXiv e-prints, arXiv:2105.00697. https://arxiv.org/abs/2105.00697

Péroux, C., Bouché, N., Kulkarni, V. P., York, D. G., & Vladilo, G. 2011, MNRAS, 410, 2251, doi: 10.1111/j.1365-2966.2010.17597.x

—. 2012, MNRAS, 419, 3060, doi: 10.1111/j.1365-2966.2011.19947.x

Péroux, C., & Howk, J. C. 2020, ARA&A, 58, 363, doi: 10.1146/annurev-astro-021820-120014

Pettini, M., King, D. L., Smith, L. J., & Hunstead, R. W. 1997, ApJ, 478, 536, doi: 10.1086/303826

Pettini, M., Zych, B. J., Steidel, C. C., & Chaffee, F. H. 2008, MNRAS, 385, 2011, doi: 10.1111/j.1365-2966.2008.12951.x

Pieri, M. M., Bonoli, S., Chaves-Montero, J., et al. 2016, in SF2A-2016: Proceedings of the Annual meeting of the French Society of Astronomy and Astrophysics, ed. C. Reylé, J. Richard, L. Cambrésy, M. Deleuil, E. Pécontal, L. Tresse, & I. Vauglin, 259–266. https://arxiv.org/abs/1611.09388

Rafelski, M., Neeleman, M., Fumagalli, M., Wolfe, A. M., & Prochaska, J. X. 2014, ApJ, 782, L29, doi: 10.1088/2041-8205/782/2/L29

Rafelski, M., Wolfe, A. M., Prochaska, J. X., Neeleman, M., & Mendez, A. J. 2012, ApJ, 755, 89, doi: 10.1088/0004-637X/755/2/89

Ranjan, A., Noterdaeme, P., Krogager, J. K., et al. 2020, A&A, 633, A125, doi: 10.1051/0004-6361/201936078

Robert, P. F., Murphy, M. T., O'Meara, J. M., Crighton, N. H. M., & Fumagalli, M. 2019, MNRAS, 483, 2736, doi: 10.1093/mnras/sty3287

Roederer, I. U., Preston, G. W., Thompson, I. B., et al. 2014, AJ, 147, 136, doi: 10.1088/0004-6256/147/6/136

Ryan, S. G., Norris, J. E., & Beers, T. C. 1996, ApJ, 471, 254, doi: 10.1086/177967

Ryan, S. G., Norris, J. E., & Bessell, M. S. 1991, AJ, 102, 303, doi: 10.1086/115878

Salvadori, S., & Ferrara, A. 2009, MNRAS, 395, L6, doi: 10.1111/j.1745-3933.2009.00627.x

Simcoe, R. A., Sullivan, P. W., Cooksey, K. L., et al. 2012, Nature, 492, 79, doi: 10.1038/nature11612

Simon, J. D. 2019, ARA&A, 57, 375, doi: 10.1146/annurev-astro-091918-104453

Simon, J. D., Geha, M., Minor, Q. E., et al. 2011, ApJ, 733, 46, doi: 10.1088/0004-637X/733/1/46

Skidmore, W., TMT International Science Development Teams, & Science Advisory Committee, T. 2015, Research in Astronomy and Astrophysics, 15, 1945, doi: 10.1088/1674-4527/15/12/001

Stacy, A., Bromm, V., & Lee, A. T. 2016, MNRAS, 462, 1307, doi: 10.1093/mnras/stw1728

Starkenburg, E., Martin, N., Youakim, K., et al. 2017, MNRAS, 471, 2587, doi: 10.1093/mnras/stx1068

Tegmark, M., Silk, J., Rees, M. J., et al. 1997, ApJ, 474, 1, doi: 10.1086/303434

Trussler, J. A. A., Conselice, C. J., Adams, N. J., et al. 2022, arXiv e-prints, arXiv:2211.02038. https://arxiv.org/abs/2211.02038

Turk, M. J., Abel, T., & O'Shea, B. 2009, Science, 325, 601, doi: 10.1126/science.1173540

van der Walt, S., Colbert, S. C., & Varoquaux, G. 2011, Computing in Science and Engineering, 13, 22, doi: 10.1109/MCSE.2011.37

Vladilo, G., Abate, C., Yin, J., Cescutti, G., & Matteucci, F. 2011, A&A, 530, A33, doi: 10.1051/0004-6361/201016330

Vogt, S. S., Allen, S. L., Bigelow, B. C., et al. 1994, in Society of Photo-Optical Instrumentation Engineers (SPIE) Conference Series, Vol. 2198, Instrumentation in Astronomy VIII, ed. D. L. Crawford & E. R. Craine, 362, doi: 10.1117/12.176725

Walker, M. G., Mateo, M., Olszewski, E. W., et al. 2016, ApJ, 819, 53, doi: 10.3847/0004-637X/819/1/53

Welsh, L., Cooke, R., & Fumagalli, M. 2019, MNRAS, 487, 3363, doi: 10.1093/mnras/stz1526

Welsh, L., Cooke, R., Fumagalli, M., & Pettini, M. 2020, MNRAS, 494, 1411, doi: 10.1093/mnras/staa807

—. 2022, ApJ, 929, 158, doi: 10.3847/1538-4357/ac4503

Wolfe, A. M., Gawiser, E., & Prochaska, J. X. 2005, ARA&A, 43, 861, doi: 10.1146/annurev.astro.42.053102.133950

Wolfe, A. M., Turnshek, D. A., Smith, H. E., & Cohen, R. D. 1986, ApJs, 61, 249, doi: 10.1086/191114

Woosley, S. E. 2017, ApJ, 836, 244, doi: 10.3847/1538-4357/836/2/244

Woosley, S. E., & Weaver, T. A. 1995, ApJS, 101, 181, doi: 10.1086/192237

Zou, S., Petitjean, P., Noterdaeme, P., et al. 2020, ApJ, 901, 105, doi: 10.3847/1538-4357/abb092